The K_2 $2^3\Pi_g$ State: New Observations and Analysis

F. Xie, D. Li, Y. Chu, and Li Li*

Department of Physics and Key Laboratory of Atomic and Molecular Nanosciences, Tsinghua University, Beijing 100084, China

S. Magnier

Laboratoire des Atomes, Lasers, Mole'cules et Surfaces (PALMS), CNRS et Universite' RENNES I (UMR 6627), Campus de Beaulieu, Bt 11B 35042 Rennes Cedex, France

V. B. Sovkov and V. S. Ivanov

V. A. Fock Institute of Physics, St. Petersburg State University, 1 Ulyanovskaya Street, Petrodvorets, St. Petersburg 198504, Russia

Received: May 27, 2006; In Final Form: July 19, 2006

Totally 3045 transitions into the $2^3\Pi_g$ $v = 0-42$, $J = 0-103$, $\Omega = 0$, 1, 2 rovibrational levels have been observed by infrared−infrared double resonance fluorescence excitation and two-photon spectroscopy. Molecular constants including the spin−orbit interaction parameters are obtained. Although the K_2 $2^3\Pi_g$ state dissociates to the 4s + 3d atomic limit, it is strongly mixed with the ^{3}P ionic states in the range of the potential well. This mixing results in a relatively large equilibrium internuclear distance $R_e = 5.254$ Å and a larger spin−orbit constant $A_0 \sim 14.17$ cm^{-1} than that of the atomic limit −2.33 cm^{-1}. Strong perturbations of the $2^3\Pi_g$ levels observed are attributed to the spin−orbit coupling with the $4^1\Sigma_g^+$ state.

1. Introduction

The $2^3\Pi_g$ state of alkali metal dimers has received much attention both experimentally and theoretically.[1−8] This state has a relatively large equilibrium internuclear distance, R_e, and exhibits strong fluorescence to the lowest triplet state $a^3\Sigma_u^+$. Although the $2^3\Pi_g$ state of the Na_2 and Li_2 molecules was observed[3,9−11] 20 years ago by the perturbation facilitated optical−optical double resonance (PFOODR) excitation spectroscopy via the $A^1\Sigma_u^+\sim b^3\Pi_u$ mixed intermediate window levels, the $2^3\Pi_g$ state of the K_2 molecule was observed much later because of experimental difficulties (two infrared lasers are required to reach this state in K_2, in place of the visible and near-ultraviolet lasers in the case of Na_2 and Li_2). Besides, the accurate molecular constants of the $A^1\Sigma_u^+$ and $b^3\Pi_u$ states of the K_2 molecule had become available only recently.[12] The observations of the $v = 4-14$, $\Omega = 0$, 1 levels of the K_2 $2^3\Pi_g$ state by perturbation facilitated infrared−infrared (IR−IR) double resonance and two-photon $2^3\Pi_g \leftarrow X^1\Sigma_g^+$ spectroscopy (101 transitions total) along with the corresponding analysis were reported.[13] The strong $2^3\Pi_g \rightarrow a^3\Sigma_u^+$ fluorescence spectrum, peaking at 573 nm, was used to determine the potential energy curve of the K_2 $a^3\Sigma_u^+$ state.[14]

At the moment we have observed many more vibrational−rotational levels of the $^{39}K_2$ $2^3\Pi_g$ state (3045 transitions total), including the $v = 0-3$ levels and the $\Omega = 2$ component. The current paper reports the new observations and their analysis. The data on the $^{39}K_2$ $4^1\Sigma_g^+$ state, obtained in a similar experiment, and the deperturbation of the $2^3\Pi_g \sim 4^1\Sigma_g^+$ mixed levels will be published separately.

2. Experimental Techniques

The experimental details were described in ref 13. Briefly, potassium vapor was generated in a heatpipe oven at 300 °C with 1 Torr argon buffer gas. Two single-mode tunable Toptica DL 100 diode lasers were used as the pump and probe lasers. The pump laser selectively excited an $A^1\Sigma_u^+\sim b^3\Pi_u$ mixed intermediate level and the probe laser frequency was scanned. The IR−IR double resonance signals of the $2^3\Pi_g$ state were detected by monitoring the $2^3\Pi_g \rightarrow a^3\Sigma_u^+$ yellow-green fluorescence. A Spex 1404 monochromator was used to resolve the fluorescence from the $2^3\Pi_g$ state.

3. Observations

Accurate molecular constants of the intermediate $A^1\Sigma_u^+$ and $b^3\Pi_u$ states as well as of the ground $X^1\Sigma_g^+$ state were reported in refs 12 and 15 correspondingly. With these constants, pump transition frequencies from the ground-state levels into the $A^1\Sigma_u^+\sim b^3\Pi_u$ mixed levels can be predicted with the accuracy better than 0.08 cm^{-1}. Since the $A^1\Sigma_u^+$ and $b^3\Pi_u$ states strongly perturb each other, many $A^1\Sigma_u^+\sim b^3\Pi_{\Omega'u}$ ($\Omega' = 0$, 1) mixed levels have been used as the intermediate window levels for double resonance excitation into triplet states. We also found five $A^1\Sigma_u^+\sim b^3\Pi_{\Omega'u}$ $\Omega' = 2$ mixed levels, which have been used as the intermediate window levels to observe the $2^3\Pi_g$ $\Omega = 2$ levels.

The Doppler linewidth of $^{39}K_2$ at 300 °C is about 0.02 cm^{-1}. To set the pump laser frequency at the Doppler line center, we first tuned the pump laser frequency to the predicted frequency

* To whom all correspondences should be addressed. Phone: 86-10-6278-8938, ext 155. FAX: 86-10-6278-1598. E-mail: lili@mail.tsinghua.edu.cn.

10.1021/jp063266m CCC: $33.50
Published on Web 09/12/2006

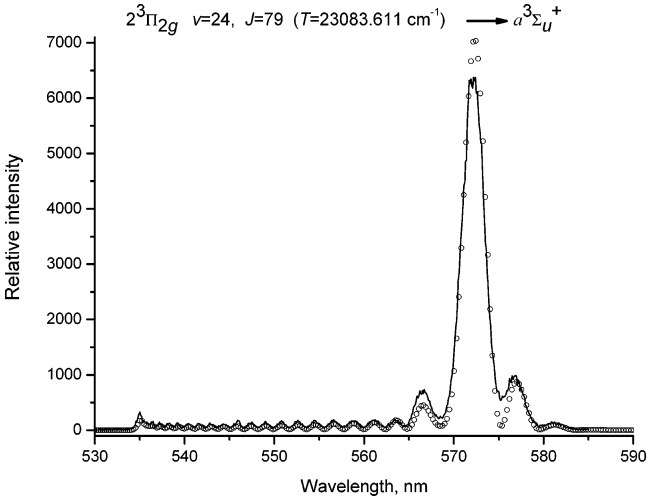

Figure 1. Resolved fluorescence of the $^{39}K_2$ $2^3\Pi_{2g}$ $v = 24$, $J = 79 \rightarrow a^3\Sigma_u^+$ transition: experimental (solid line) and simulated (circles). The fragment of the spectrum at $\lambda < 536.7$ nm is the fluorescence into the bound levels of the $a^3\Sigma_u^+$ state that are not resolved in the figure.

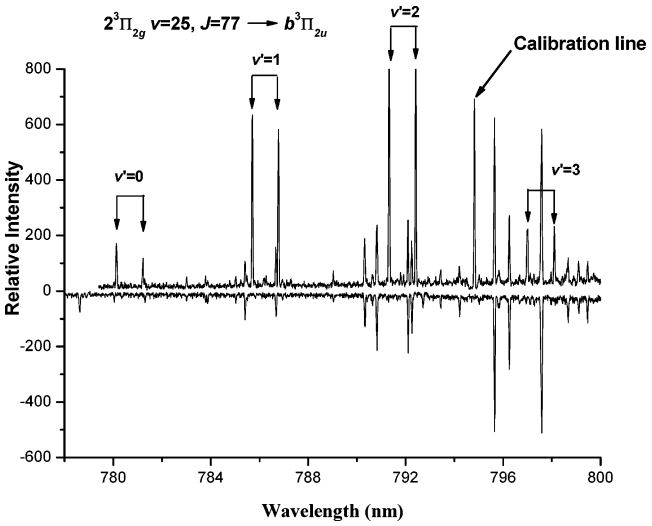

Figure 2. Resolved fluorescence of the $^{39}K_2$ $2^3\Pi_{2g}$ $v = 25$, $J = 77 \rightarrow b^3\Pi_{2u}$ transition. The upper spectrum was recorded when the pump (11 732.215 cm^{-1}) and probe (10 652.772 cm^{-1}) lasers excited the $2^3\Pi_{2g}$ $v = 25$, $J = 77 \leftarrow b^3\Pi_{2u}$ $v' = 25$, $J' = 78 \leftarrow X^1\Sigma_g^+$ $v'' = 4$, $J'' = 77$ transition. The lower spectrum was recorded without the probe laser. Fluorescence lines from the $2^3\Pi_{2g}$ $v = 25$, $J = 77$ level into the $b^3\Pi_{2u}$ $v' = 0-3$ vibrational levels are assigned in the upper spectrum.

and scanned the probe laser frequency to find a double resonance signal and then adjusted the pump laser frequency up−down with a 0.002 cm^{-1} step and repeated the probe laser frequency scan to optimize the double resonance signal. When the signal was the strongest, the pump laser frequency was at the Doppler line center of the pump transition and held fixed there.

Figure 1 displays one of the resolved fluorescence spectra measured in the experiment, namely, the $2^3\Pi_{2g}$ $v = 24$, $J = 79 \rightarrow a^3\Sigma_u^+$ transition, along with its simulation (see the section "Analysis" below). The part of the spectrum at $\lambda \leq 536.7$ nm is the fluorescence into the bound levels of the shallow well of the $a^3\Sigma_u^+$ state (unresolved in Figure 1).

Figure 2 shows the resolved fluorescence in the 778−800 nm region when the pump (11 732.215 cm^{-1}) and the probe (10 652.772 cm^{-1}) lasers excited the $2^3\Pi_{2g}$ $v = 25$, $J = 77 \leftarrow b^3\Pi_{2u}$ $v' = 25$, $J' = 78 \leftarrow X^1\Sigma_g^+$ $v'' = 4$, $J'' = 77$ transition. Besides the $2^3\Pi_{2g}$ $v = 25$, $J = 77 \rightarrow b^3\Pi_{2u}$ $v' = 0-3$ fluorescence lines, many additional lines appear in the spectrum.

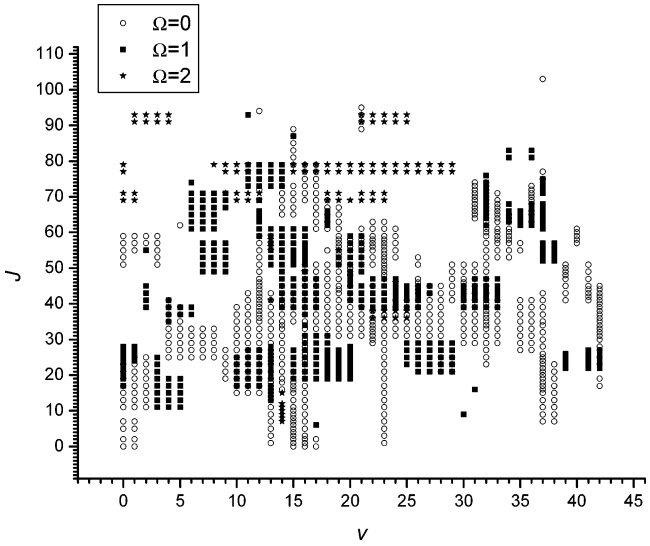

Figure 3. Data field of the $^{39}K_2$ $2^3\Pi_g$ state rovibrational levels observed by the IR−IR double resonance excitation.

Although the pump and probe laser frequencies were in the frequency range of the $A^1\Sigma_u^+ \leftarrow X^1\Sigma_g^+$ transitions, the $A^1\Sigma_u^+ \rightarrow X^1\Sigma_g^+$ fluorescence would have much longer wavelength. The lower spectrum was recorded when the probe laser was blocked. Because the density of the accessible rovibronic levels of K_2 was high under our experimental conditions, the pump laser itself excited a two-photon transition and gave rise to a fluorescence in this wavelength region.[13] The probe laser itself did not induce a fluorescence in this wavelength region.

On the whole, 2944 new IR−IR double resonance transitions into levels of the K_2 $2^3\Pi_g$ state have been observed and assigned (Appendix A, Supporting Information) in addition to 101 double resonance and two-photon transitions reported in ref 13. The newly observed levels span a greater range of the vibrational quantum number ($v = 0-42$ in place of $v = 4-14$) and the rotational quantum number ($J = 0-103$ in place of $J = 19-41$). The levels observed in ref 13 belonged only to $\Omega = 0$ and $\Omega = 1$ components, while the new data include 211 transitions to the $\Omega = 2$ component. Figure 3 shows the $v-J$ distributions of the three Ω components.

4. Analysis

The $2^3\Pi_g$ state has case a coupling at low J with a spin−orbit splitting of ∼14 cm^{-1}.[13] Using the $^3\Pi_0$, $^3\Pi_1$, $^3\Pi_2$ case a basis, the effective Hamiltonian matrix elements are[16]

$$\langle {}^3\Pi_0, v, J|H|{}^3\Pi_0, v, J\rangle = T_e + G_v + B_v(X+1) - D_v(X^2+4X+1) - \tilde{A}_v$$

$$\langle {}^3\Pi_1, v, J|H|{}^3\Pi_1, v, J\rangle = T_e + G_v + B_v(X+1) - D_v(X^2+6X-3)$$

$$\langle {}^3\Pi_2, v, J|H|{}^3\Pi_2, v, J\rangle = T_e + G_v + B_v(X-3) - D_v(X^2-4X+5) + \tilde{A}_v$$

$$\langle {}^3\Pi_0, v, J|H|{}^3\Pi_1, v, J\rangle = -(2X)^{1/2}[B_v - 2(X+1)D_v]$$

$$\langle {}^3\Pi_0, v, J|H|{}^3\Pi_2, v, J\rangle = -2D_v[X(X-2)]^{1/2}$$

$$\langle {}^3\Pi_1, v, J|H|{}^3\Pi_2, v, J\rangle = -(2X-4)^{1/2}[B_v - 2D_v(X-1)]$$

where $X = J(J+1)$.

TABLE 1: Molecular Constants of the $^{39}K_2$ $2^3\Pi_g$ State[a]

	this work	ab initio[8]
$T_e + Y_{00}$	21 601.740 7(16 6)	21 583
Y_{10}	55.017 891 (13 517)	53.40
Y_{20}	−0.169 836 2(3 679 7)	
Y_{30}	0.005 304 245 (443 247)	
Y_{40}	−3.156 548 (272 688) × 10^{-4}	
Y_{50}	1.074 823 0(89 488 0) × 10^{-5}	
Y_{60}	−1.898 627 (149 138) × 10^{-7}	
Y_{70}	1.341 395 (99 188) × 10^{-9}	
Y_{01}	0.031 348 83(7 16)	0.031 3
Y_{11}	4.739 2(81 0) × 10^{-5}	
Y_{21}	−2.214 24(46 82) × 10^{-6}	
Y_{31}	1.893 9(80 4) × 10^{-8}	
Y_{02}	−4.100 2(80 5) × 10^{-8}	
Y_{12}	−1.013 3(40 0) × 10^{-9}	
A_0	14.168 2(4 4)	
A_2	−6.362 (69) × 10^{-4}	
R_e (Å)	5.253 8	5.26
Y_{00}	−0.040 0	

[a] Measurement units are cm^{-1} and angstrom. The value of A_1 is statistically insignificant.

All v-dependent constants of the above equations have been represented by the Dunham-like polynomial expressions

$$G_v = \sum_{i=0} Y_{i0}(v + 1/2)^i$$

$$B_v = \sum_{i=0} Y_{i1}(v + 1/2)^i$$

$$D_v = -\sum_{i=0} Y_{i2}(v + 1/2)^i$$

$$\tilde{A}_v = \sum_{i=0} A_i(v + 1/2)^i$$

By numerically diagonalizing the resulting matrix for each v, J and performing a nonlinear least-squares fit to the entire set of the observed unperturbed terms, the values of Y_{ij} and A_i have been obtained. The resulting values are presented in Table 1 along with the ab initio estimates reported in ref 8. The final value $D_e = -Y_{02} = 4.10 \times 10^{-8}$ cm^{-1} is very close to the semiclassical estimate[17] $4B_e^3/\omega_e^2 = 4Y_{01}^3/Y_{10}^2 = 4.07 \times 10^{-8}$ cm^{-1}, confirming that the result is self-consistent.

The RKR curve computed from the constants of Table 1 is presented in Table 2.

As an independent check of the quality of the results we have simulated the experimental fluorescence spectra of the $2^3\Pi_g \rightarrow a^3\Sigma_u^+$ transitions. To do that we have implemented the split-operator computational technique[18−20] and used the RKR potential functions of the $2^3\Pi_g$ state constructed from the molecular constants of this work, the modified Lennard-Jones (MLJ)[21] potential function of the $a^3\Sigma_u^+$ state from ref 14, and the ab initio[7,8] dipole moment function of the $2^3\Pi_g \rightarrow a^3\Sigma_u^+$ transition. All the simulated spectra have reproduced the experimental ones with a reasonably good accuracy. As an example, the simulation of the $2^3\Pi_{2g}$ $v = 24$, $J = 79 \rightarrow a^3\Sigma_u^+$ fluorescence is shown in Figure 1 along with the experimental spectrum.

Due to perturbations some part of the experimental term values could not be fitted with a satisfactory accuracy. Those outliers have been excluded from the fit in a following procedure: (i) an initial set of the term values has been fitted, (ii) the averaged standard deviation σ of the calculated and experimental term values has been estimated, (iii) those term values that had deviated by more than 3σ have been excluded from the initial set (and are designated "perturbed"), and (iv) the procedure has been iterated until all the remaining term values are within the range of $\pm 3\sigma$ (and are designated "unperturbed"). The resulting errors of the reproduction of the remaining "unperturbed" term values are shown in Figure 4. Their histogram is compared with the normal distribution density in Figure 5. No significant systematic errors can be observed.

The "perturbed" values excluded from the fit are a set of 446, including 397 transitions to the $\Omega = 0$ component, 39 transitions to the $\Omega = 1$ component, and 10 transitions to the $\Omega = 2$ component. Their deviations from the approximate values based on molecular constants are shown in Figure 6. Many of these deviations exhibit a characteristic behavior of resonantly perturbed terms. As the majority of the perturbed terms belong to the $\Omega = 0$ component, it can be concluded from the selection rules that the main perturber is a state of the $^1\Sigma_g^+$ symmetry. Obviously, it is the $4^1\Sigma_g^+$ state, whose levels have been also observed by us in the same energy range. Results of the analysis

TABLE 2: RKR Potential Curve of the K_2 $2^3\Pi_g$ State with the Constants of Table 1[a]

R_{min}	R_{max}	$T_e + G_v$	v	R_{min}	R_{max}	$T_e + G_v$	v
5.078 03	5.432 93	21 629.207 78	0	4.137 97	6.625 74	22 774.445 06	22
4.950 84	5.567 32	21 683.901 74	1	4.115 88	6.663 20	22 823.802 92	23
4.864 04	5.661 79	21 738.295 45	2	4.094 40	6.700 34	22 872.933 56	24
4.794 01	5.739 98	21 792.408 13	3	4.073 47	6.737 18	22 921.836 94	25
4.733 86	5.808 74	21 846.254 19	4	4.053 07	6.773 75	22 970.512 61	26
4.680 47	5.871 18	21 899.844 20	5	4.033 16	6.810 08	23 018.959 64	27
4.632 08	5.929 06	21 953.185 63	6	4.013 71	6.846 19	23 067.176 71	28
4.587 58	5.983 46	22 006.283 58	7	3.994 69	6.882 12	23 115.162 13	29
4.546 24	6.035 11	22 059.141 39	8	3.976 07	6.917 87	23 162.913 99	30
4.507 53	6.084 53	22 111.761 08	9	3.957 84	6.953 47	23 210.430 28	31
4.471 05	6.132 12	22 164.143 81	10	3.939 96	6.988 94	23 257.709 18	32
4.436 50	6.178 16	22 216.290 20	11	3.922 42	7.024 28	23 304.749 30	33
4.403 63	6.222 88	22 268.200 62	12	3.905 20	7.059 50	23 351.550 11	34
4.372 27	6.266 47	22 319.875 31	13	3.888 29	7.094 60	23 398.112 39	35
4.342 24	6.309 08	22 371.314 62	14	3.871 69	7.129 58	23 444.438 75	36
4.313 42	6.350 83	22 422.519 02	15	3.855 39	7.164 42	23 490.534 32	37
4.285 70	6.391 82	22 473.489 16	16	3.839 39	7.199 08	23 536.407 48	38
4.258 98	6.432 13	22 524.225 89	17	3.823 71	7.233 52	23 582.070 71	39
4.233 19	6.471 84	22 574.730 20	18	3.808 37	7.267 68	23 627.541 59	40
4.208 25	6.511 00	22 625.003 19	19	3.793 39	7.301 47	23 672.843 89	41
4.184 11	6.549 68	22 675.045 98	20	3.778 81	7.334 81	23 718.008 80	42
4.160 70	6.587 91	22 724.859 64	21	3.764 68	7.367 55	23 763.076 30	43

[a] $R_e = 5.2538$ Å, $T_e = 21\,601.781$ cm^{-1}, $v_{min} = -0.49927$, $Y_{00} = -0.0400$ cm^{-1}.

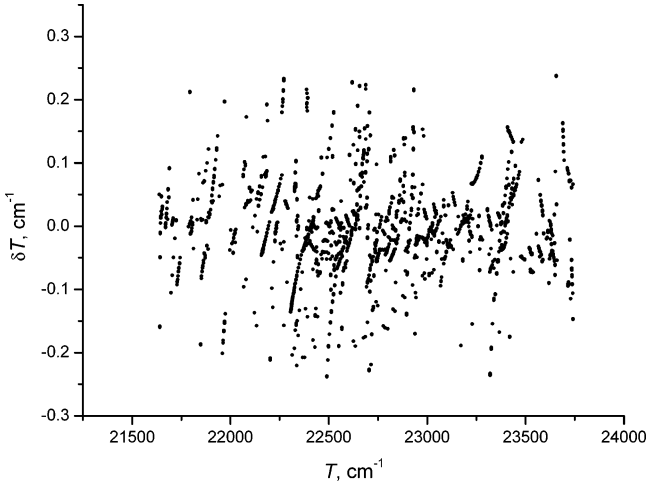

Figure 4. Errors in reproducing "unperturbed" experimental term values of the $^{39}K_2$ $2^3\Pi_g$ state with the molecular constants determined in the current work.

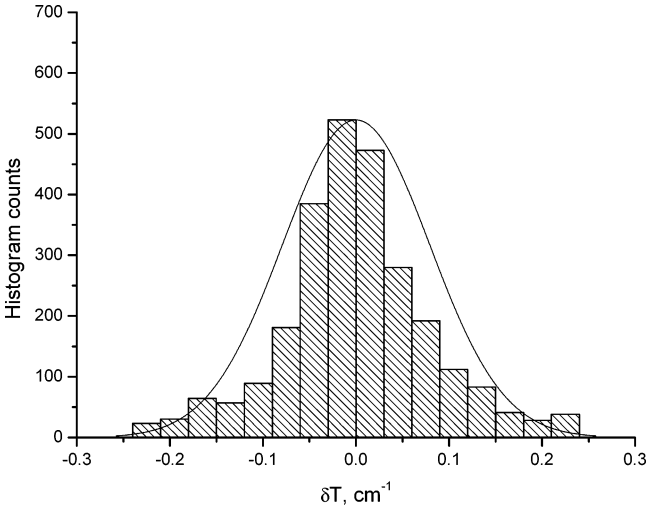

Figure 5. Histogram of the errors of the unperturbed experimental term values of the $^{39}K_2$ $2^3\Pi_g$ state reproduction with the molecular constants determined in the current work compared with the probability density of the corresponding normal distribution.

of the $4^1\Sigma_g^+$ state and the deperturbation of the $4^1\Sigma_g^+ \sim 2^3\Pi_g$ spin−orbit interaction will be published separately.

5. Discussion

Figure 7 shows the ab initio K_2 $2^3\Pi_g$ potential curve intersecting with several curves of the ionic ^3P states. Important configurations in the electronic wave function of the $2^3\Pi_g$ state include 4s4p, 4s5p, 4s6p, and 4s7p. The analysis based on the ab initio computations[8] shows that the K_2 $2^3\Pi_g$ state between 3.5 Å (7 au) and 6.5 Å (13 au) is built mainly from the ionic 4p7p and covalent 6p3d configurations, and in this range it can be considered as an ionic state.

Three experimental observations testify to this inference. (i) The K_2 $2^3\Pi_g$ state dissociates to the 4s + 3d atomic limit. The $\sim$14.17 cm^{-1} spin−orbit constant of the $2^3\Pi_g$ state is much larger than the spin−orbit splitting of the 3d atom, −2.33 cm^{-1}. (ii) The dependence of the rotational constant B_v on the vibrational quantum number v has a nontrivial nonmontonic character (see Figure 8). The standard deviations shown in the same figure confirm that this behavior is statistically significant. In our opinion, such an unusual dependence suggests that the K_2 $2^3\Pi_g$ electronic state configuration changes with the internuclear distance. (iii) A relatively large equilibrium internuclear distance $R_e \sim 5.25$ Å can also be explained by mixing the covalent 6p3d and ionic configurations. Calculations on ionic resonance states of K^- and their influence on potential energy curves of K_2 molecular states will be published separately.

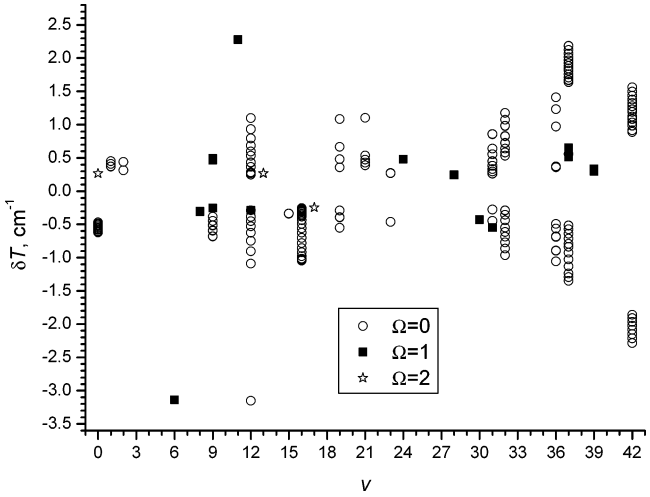

Figure 6. Errors in reproducing "perturbed" experimental term values of the $^{39}K_2$ $2^3\Pi_g$ state with the molecular constants determined in the current work.

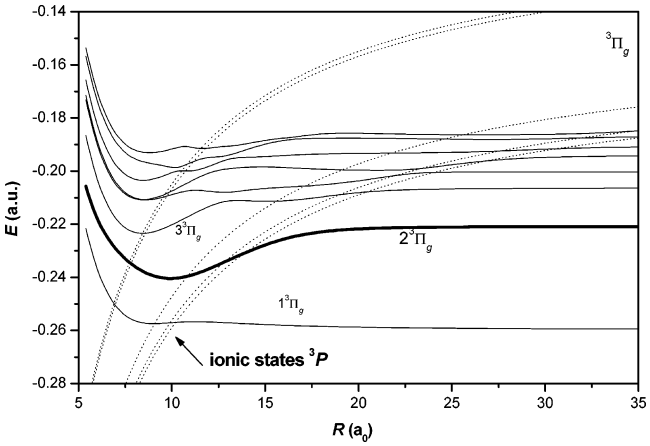

Figure 7. Influence of the potential energy curves of the ionic ^3P states (dissociating to the $K^+ + K^-$ ($^3P(n\ell n'\ell')$ limits) on potential energy curves of the $^3\Pi_g$ states of K_2 from the K(4s) + K(4p) limits up to the K(4s) + K(5d) limits at intermediate and large R.

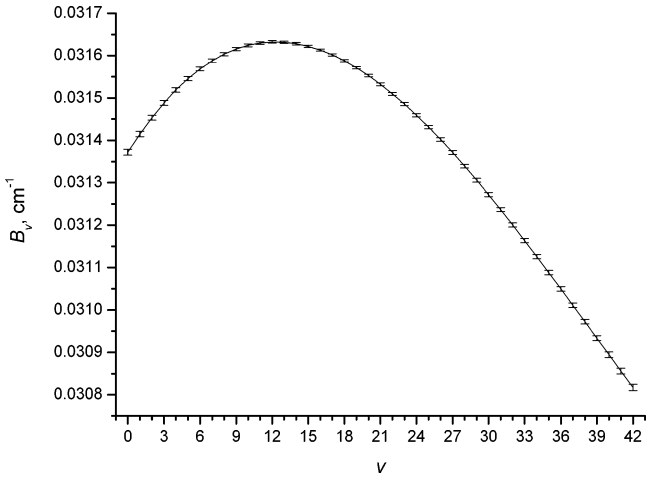

Figure 8. Rotational constant B_v of the $^{39}K_2$ $2^3\Pi_g$ state vs the vibrational quantum number v. Standard deviations computed from the estimated covariance matrix of the Y_{i1} values are also shown.

Acknowledgment. We thank Prof. T. Bergeman for calculating the term values of the intermediate levels. Support from the NSFC (20473042), NKBRSF, and SRFDP of China as well as from the RFBR (05-03-39012) of Russia are gratefully acknowledged.

Supporting Information Available: Data of the K_2 $2^3\Pi_g$ state by infrared−infrared double resonance: Intermediate levels, probe transition frequencies, the v, J, Ω assignments, and term values of the $2^3\Pi_g$ state. This material is available free of charge via the Internet at http://pubs.acs.org.

References and Notes

(1) Li, L.; Field, R. W. *J. Phys. Chem.* **1983**, *87*, 3020−3022.

(2) Li, L.; Field, R. W. CW Perturbation Facilitated Optical-Optical Double Resonance (PFOODR) Spectroscopy of Na_2 and Li_2. In *Molecular Spectroscopy and Dynamics by Stimulated Emission Pumping;* Dai, H. L., Field, R. W., Eds.; World Scientific: Singapore, 1995; Chapter 7.

(3) Pichler, G.; Bahns, J. T.; Sando, K.; Stwalley, W. C.; Konowalow, D. D.; Li, L.; Field, R. W.; Muller, W. *Chem. Phys. Lett.* **1986**, *129*, 425−428.

(4) Li, L.; Lyyra, A. M. *Spectrochim. Acta Part A* **1999**, *55A*, 2147−2178 and the references therein.

(5) Konowalow, D. D.; Rosenkrantz, M. E.; Olson, M. L. *Chem. Phys.* **1980**, *72*, 2612−2615.

(6) Schmidt-Mink, I.; Mueller, W.; Meyer, W. *Chem. Phys.* **1985**, *92*, 263−285.

(7) Magnier, S.; Millie, Ph. *Phys. Rev. A.* **1996**, *54*, 204−218.

(8) Magnier, S.; Aubert-Frecon, M.; Allouche, A. R. *J. Chem. Phys.* **2004**, *121*, 1771−1781.

(9) Li, L.; Field, R. W. *J. Mol. Spectrosc.* **1986**, *117*, 245−282.

(10) Xie, X.; Field, R. W. *J. Mol. Spectrosc.* **1986**, *117*, 228−244.

(11) Li, L.; Rice, S. F.; Field, R. W. *J. Chem. Phys.* **1985**, *82*, 1178−1182.

(12) Manaa, M. R.; Ross, A. J.; Martin, F.; Crozet, P.; Lyyra, A. M.; Li, L.; Amiot, C.; Bergeman, T. *J. Chem. Phys*. **2002**, *117*, 11208−11215 and the references therein.

(13) Chu, Y.; Xie, F.; Li, D.; Li, L.; Sovkov, V. B.; Ivanov, V. S.; Lyyra, A. M. *J. Chem. Phys.* **2005**, *122*, 074302(1−8).

(14) Ahmed, E.; Lyyra, A. M.; Xie, F.; Li, D.; Chu, Y.; Li, L.; Ivanov, V. S.; Sovkov, V. B.; Magnier, S. *J. Mol. Spectrosc*. **2005**, *234*, 41−52.

(15) Heinze, J.; Schuhle, U.; Engelke, F.; Caldwell, C. D. *J. Chem. Phys.* **1987**, *87*, 45−53.

(16) Kovács, I. *Rotational Structure in the Spectra of Diatomic Molecules*, Hilger: London, 1969.

(17) Lefebvre-Brion H.; Field, R. W. *The Spectra and Dynamics of Diatomic Molecules;* Elsevier: New York, 2004.

(18) Feit, M. D.; Fleck, J. A., Jr. *J. Chem. Phys.* **1983**, *78*, 301−308.

(19) Alvarellos, J.; Metiu, H. *J. Chem. Phys.* **1988**, *88*, 4957−4966.

(20) Serov, V. N.; Sovkov, V. B.; Ivanov, V. S.; Atabek, O. *J. Chem. Phys.* **2001**, *115*, 6450−6458.

(21) Hajigeorgiou, Ph. G.; Le Roy, R. J. *J. Chem. Phys.* **2000**, *112*, 3949−3957.